Conference Paper

Computational Study of Two-Phase Flow Morphology in a Nozzle

Balakin B. V.[1,2], Kuzmenkov D. M.[2], Kutsenko K. V.[2], Maslov Yu. A.[2], Saparbaeva N. A.[2], and Kharitonov V. S.[2]

[1]Western Norway University of Applied Sciences, Bergen, Norway
[2]National Research Nuclear University MEPhI (Moscow Engineering Physics Institute), Kashirskoe shosse 31, Moscow, 115409, Russia

Abstract

Multiphase flow meters are widely used in nuclear, petroleum and chemical industries. Here the flow rate is defined indirectly by the differential pressure measurement over the device. An additional measurement is required to estimate average density of the phase mixture. This could be done by means of the gamma-ray, electromagnetic or acoustic tomography. The accuracy of the technique is dependent on flow morphology. The present paper reports the results of CFD-modelling of the gas-liquid flow through the vertical flow meter accompanied by a flow conditioner. The model is used to consider the morphology for three different combinations of liquid and gas flow rates. The model demonstrates high non-uniformities of the flow field at the entrance of the flow meter and generally confirms the agreement of flow morphology with previous experimental observations for vertical pipes.

Keywords: CFD, two-phase, flow morphology, STAR-CCM+, flowmeter

Corresponding Author:
Balakin B. V.
Boris.Balakin@hvl.no

Received: 23 December 2017
Accepted: 15 January 2018
Published: 21 February 2018

Publishing services provided by Knowledge E

Selection and Peer-review under the responsibility of the AtomFuture Conference Committee.

1. Introduction

Multiphase flow consists of several chemically immiscible materials [2, 4], flows of this type are frequently utilized nuclear, petroleum and chemical industries. Among the in-line measurement systems, the multiphase flow measurement represents the most significant emergent technology in the last two decades. The technology is based on the definition of the flow rate of each phase which comes through a multiphase flow meter. The differential pressure measurement over the Venturi nozzle, orifice or V-cone is most-commonly utilized for the estimation of flow rate of all the phases (ISO 5167:2003), i.e. total flow rate. Basing on the total flow measurement, the flow rate for each separate phase can be estimated with the use of additional measurement. This measurement allows determination of phase volume fraction; gamma-ray densitometry, sampling, electromagnetic or acoustic tomography are applicable here.

It is usually suggested that the pressure profile across the flowmeter would be in close proximity to the one for single phase, i.e. the flow is assumed to be homogeneous there. The flow morphology however is strongly dependent on the interphase transfer of mass, momentum and energy, especially for flow channels of complex configuration, which results in non-uniform relative distribution of phases in space [9], flow regime change due to increase in difference between gas and liquid velocities (slip ratio) (Kuo and Wallis, 1988). This leads to formation of the pressure profile that is significantly different from the one for the single phase. The pressure drop in vertical and horizontal multiphase flowmeters has been studied extensively [1, 8, 11, 14].

Malayeri et al. (2001) in their experimental work reported variation of void fraction through a vertical flowmeter at various gas-water flow rates, demonstrating high sensitivity of the flow morphology to the mutual combination of separate phase flow rates. The work however does not correlate flow morphology with the differential pressure measurements in the device. The article by Jana et al. (2008), conversely, analyses the temporal history of the pressure drops over a multiphase flowmeter. Jana et al. (2008) do not however present any explicit visual data on the flow morphology which makes their results to be limited with respect to all possible industrial conditions. An extensive experimental study has been performed by Lupeau et al. (2007) working with the two-phase flow in vertical flowmeter. The correspondence between the pressure drop measurements and the flow morphology is clarified and discussed on the paper. Although quantification of wall liquid film thickness for different flow regimes has been done, the paper lacks information on velocity and volume fraction profiles at the core of the flow and generally does not consider structure of the flow inside the device. This information is hardly extractable by means of experiment so the numerical modelling is gradually employed nowadays [9, 12, 16]. Lupeau et al. (2007), for example, derives the two-phase numerical model for the prediction of experimental liquid film profiles. The model is however limited by one dimension (axial coordinate of the device) which does not make possible to account for complex three-dimensional structure of the flow. Paladino and Maliska (2002) developed the multiphase two-fluid turbulent model for the simulation of the multiphase flow in the flowmeter. The article [12] reports preliminary results of the interphase slip velocity and relates the differential pressure over the nozzle to integrated void fractions. The model is compared to experimental data demonstrating discrepancies with experiments in terms of the pressure drop.

Based on the literature survey presented above we conclude that there is a need for the complete examination of the flow morphology in an industrial-like multiphase

flowmeter nozzle. This contribution aims the CFD model to evaluate flow morphology in a vertical flowmeter nozzle.

2. Model Description

The turbulent flow of two phases is modelled with the multiphase mixture model [15, 17]. The model, constructed in the commercial CFD-package STAR-CCM+, assumes that the flow of both phases can be described by the set of Navier-Stokes equations for the viscous flow. The continuity equation reads separately for each phase:

$$\frac{\partial\left(\varphi_k\rho_k\right)}{\partial t}+\nabla\left(\varphi_k\rho_k\vec{u}\right)=0 \tag{1}$$

where $k = l$ for liquid and $k = g$ for gas denote the phase, ρ is the phase density and u is the velocity assumed to be equal for each phase within the computational cell. The conservation of the phase volume is accounted for by:

$$\varphi_l+\varphi_g=1 \tag{2}$$

where φ is the volume fraction.

The homogeneous two-phase mixture with the phases at volume fractions φ_l and φ_g is assumed to exist within the computational cell in a way the molecular properties of the mixture are given by:

$$\begin{aligned}\rho_m&=\rho_l\varphi_l+\rho_g\varphi_g\\ \mu_m&=\mu_l\alpha_l+\mu_g\alpha_g.\end{aligned} \tag{3}$$

where ρ_l=1000 kg/m^3, μ_l=0.001 Pa · s and $\mu_g = 1.86 \cdot 10^{-5}$ Pas.

The conservation of momentum is considered for the mixture:

$$\rho_m\frac{\partial\vec{u}}{\partial t}+\rho_m\vec{u}\nabla\vec{u}=-\nabla p+\left(\mu_m+\mu_m^t\right)\Delta\vec{u}+\rho_m\vec{g}+\vec{f_c} \tag{4}$$

where p is the pressure, μ_m and μ_{mt} are molecular and turbulent viscosity, f_c is the capillary force calculated as follows:

$$\vec{f_c}=\nabla\cdot\left(\frac{\nabla\varphi_l}{\left|\nabla\varphi_l\right|}\right)\nabla\varphi_l\sigma. \tag{5}$$

The turbulent viscosity concept is used to account for the turbulent behaviour of the flow. The parameter is set to be proportional to the turbulent kinetic energy k and the rate of the energy dissipation ε (see, for example, [3]):

$$\mu_m^t=0.09\rho_m\frac{k^2}{\varepsilon} \tag{6}$$

Two transport equations for k and ε are given below:

$$\frac{\partial(\rho_m k)}{\partial t} + \nabla(\rho_m \vec{u} k) = \nabla\left(\frac{(\mu_m + \mu_m^t)}{\sigma_k}\nabla k\right) + k(G - \rho_m \varepsilon), \tag{7}$$

$$\frac{\partial(\rho_m \varepsilon)}{\partial t} + \nabla(\rho_m \vec{u} \varepsilon) = \nabla\left(\frac{(\mu_m + \mu_m^t)}{\sigma_\varepsilon}\nabla \varepsilon\right) + \frac{\varepsilon}{k}(C_1 G - C_2 \rho \varepsilon), \tag{8}$$

where

$$G = \mu_m \left(\nabla\vec{u} + \nabla\vec{u}^T\right) : \nabla\vec{u} \tag{9}$$

and

$$\sigma_\varepsilon = \frac{\kappa^2}{\left[0.3(C_1 - C_2)\right]}. \tag{10}$$

C_1 = 1.44; C_2 = 1.92; σ_k = 1.0, and κ = 0.4187 is von Karman's constant.

The three-dimensional geometry of the process is presented in Figure 1. The model includes the flowmeter nozzle, the flow conditioner of the blind-T type and a horizontal pipeline. The flowmeter consists of the confuzor part at the entrance, short cylindrical section in the throat and the diffuser nozzle at the outlet; dimensions of the flowmeter are defined according to ISO 5167:2003. The curved pipeline is located at the inlet of the model in order to mimic industrial conditions when the flow is not always fully developed at the entrance.

The geometry is discretized by 1100000 regular control volumes with the average size of 1 mm; the mesh is presented in Figure 1. The mesh-independence study was performed for the present mesh with respect to the computational cell reduction to 0.5 mm and increase to 2 mm. Following average differences in the profiles of main flow parameters (pressure, velocity, volume fraction) were observed: 2.6% for 0.5-mm vs. 1-mm and 5% for 2-mm vs. 1-mm. The present computational was therefore considered to be the most optimal from the accuracy and computational costs point of view.

Equations 1-10 were discretized spatially on the computational mesh using the upwind scheme. Euler implicit technique was used for the temporal discretization with the time 10 ms time step. The numerical solutions was based on SIMPLE [13].

The model initial conditions suggested: u = 0 m/s, relative pressure p = 0 Pa, T = 293 K, φ_l = 0, φ_g = 1. The boundary conditions included: no-slip adiabatic wall boundary with u = 0 m/s and standard wall functions ($Y+$ in the interval 70-150), the pressure outlet with the absolute pressure p = 1 bar. The inlet boundary condition assumed uniform profile of the mean flow velocity given by:

$$u_{in} = \frac{4\left(F_l + F_g\right)}{\pi d^2}, \tag{11}$$

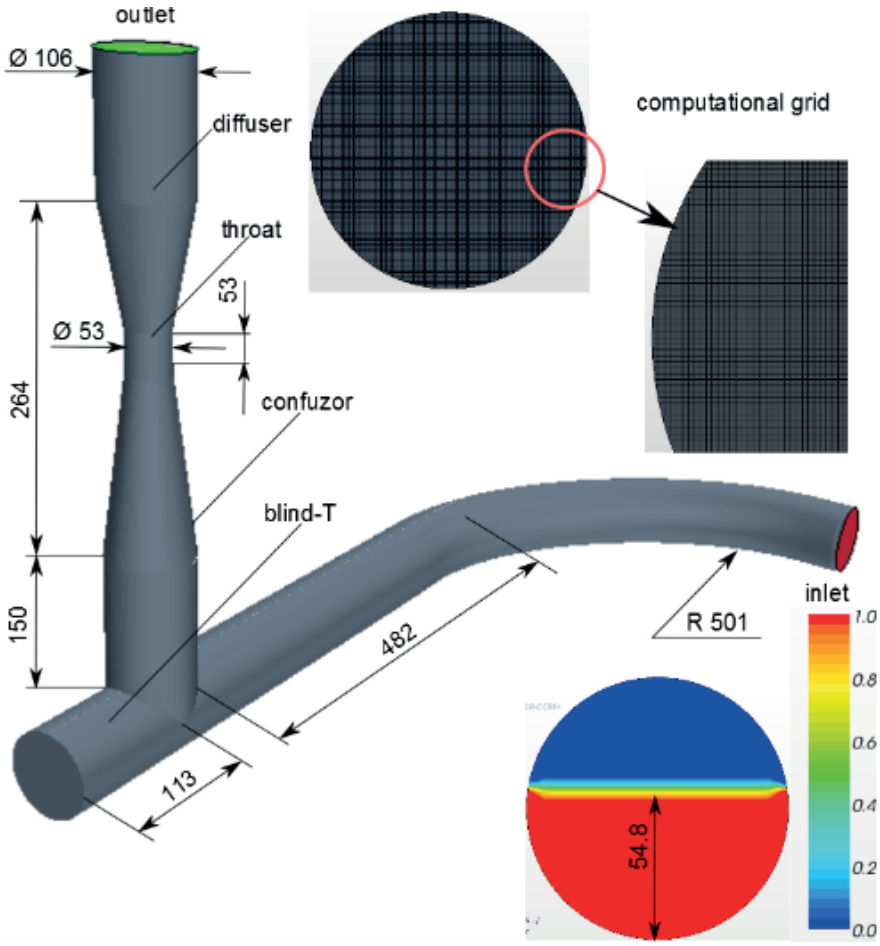

Figure 1: Three-dimensional process geometry and computational grid. Contours of water volume fraction prescribed at the inlet for regime 2. Dimensions in mm.

where *F* is the volume flow rate of each phase. The volume flow rates were selected for three different flow regimes in a manner providing notable variation of the inter-phase slip velocity and the volume fraction of phases.

Water phase is assumed being segregated at the bottom the horizontal pipeline. The corresponding cross-section of the pipe occupied by the water was equal to the average volume fraction of water from Table 1. As it is presented in Figure 1, segments of water layer with the high of 90, 55 and 7 mm for regimes 1-3 were set.

Table 1: Flow regimes.

regime	water flow rate, m^3/h	air flow rate, m^3/h	water volume fraction, %
1	8.2	0.2	92
2	24.3	0.8	60
3	10.7	218.2	3

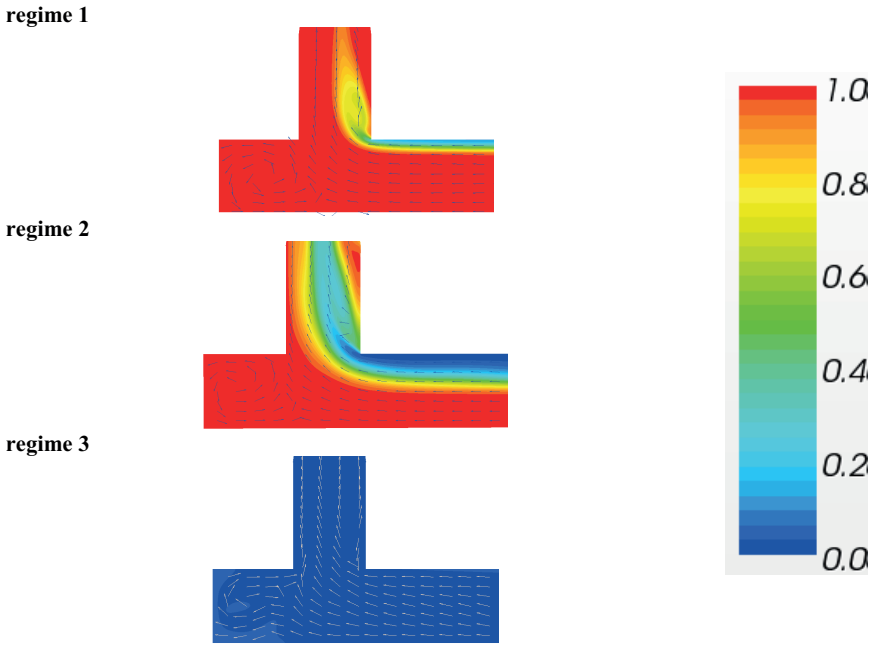

Figure 2: Time-average contours of water volume fraction together with vectors of flow velocity in the midline cross-section at the flowmeter entrance for regime 1-3. Velocity vectors are projected to the cross-sectional plane.

3. Results and Discussion

Figure 2 reports time-average contours of the water phase volume fraction together with the vectors of the flow velocity in the midline cross-section at the entrance of the system for regimes 1-3 predicted by the CFD-model. As it follows from the figure for regime 1, the gas phase does not propagate into the blind-T region due to its low inertia.

The gas flow with volume fraction up to 25% runs into the core of the flow under the angle of 50°. The air jet is shifted to the part of the confuzor which is opposite to the blind-T. The bubble flow regime is observed in the confuzor part of the flowmeter for the regime 1 that corresponds to the flow regime map for the vertical pipe [5]. Three main flow patterns are detected for the regime 1: the straight flow in the horizontal part of the system, the centralized swirl flow related to the change of the stream direction is formed in the blind-T and the vertical flow in the confuzor region. The vertical flow is slightly disturbed in the region with the maximum amount of the gas phase, i.e. the air jet due to its positive buoyancy.

The behaviour of the flow at the entrance to the flowmeter for regime 2 is characterized by significant fluidization of water phase (volume fraction in the interval 0-60%) over the upper part of the horizontal pipeline is observed. The inertia of the air stream is not enough for the formation of the steady air patterns in the blind-T. The air stream

in the confuzor occupies central part of the region with the volume fraction up to 50%, forming the flow of the annular type. The stream is slightly shifted to the zone opposite to the blind-T in a fashion similar to one observed for region 1. This shift is also characterized by an inclination of the air stream relatively to the confuzor direction what could be explained by the high inertia of the air stream. The flow patterns could be again segregated by two zones: the uni-directional flow in the horizontal pipeline, the swirl flow in the blind-T and the vertical flow in the confuzor. The vortex in the blind-T is however shifted to the upper part of the region as compared to one predicted for regime 1. The tangential flow component is observed at the entrance of the confuzor zone. The oscillations of the gaseous phase are predicted for regime 2 so the flow morphology agrees with the flow map for the vertical pipeline flow [5].

The homogeneous mist flow is observed for the regime 3 in the CFD-model. The water phase is distributed over the wall of the T-junction at the volume fractions slightly above the average value. This phenomenon could be addressed to the gravitational separation of the water phase, which is further spread by the vortex formed there. Slight non-uniformities of the flow velocity are observed at the entrance of the confuzor: the tangential component together with a counter-flow region is presented in Figure 2. As in regimes 1-2, the uni-directional flow is associated with the horizontal pipeline region.

The time-average contours of the water phase volume fraction in the midline cross-section of the entire flowmeter are presented in Figure 3 for regimes 1-3. The water phase behaviour in the vicinity of the blind-T region is illustrated in Figure 2 so here the main focus on the flow propagation through the flowmeter. It follows from the figure (regime 1) that the air occupies the region opposite to the blind-T as in the throat of the flowmeter as in the diffuser region. The complex spiralling motion of the liquid phase locates the maximum of the water volume fraction to the left part of the diffuser; the flow is not homogeneous and could be classified as the non-uniform bubble flow with the centralized liquid jet of up to 100% water volume fraction.

The water layers distributed over the confuzor region in regime 2 are further detached from the walls and dropped into the core of the flow in the throat of the flowmeter. The core of the flow is occupied by the liquid phase with the volume fraction up to 80%. The stream becomes homogenous in the vicinity of the outlet of the diffuser.

The homogeneous mist flow at the water volume fraction up to 4% is observed for the regime 3 at all the parts of the flowmeter, i.e. the water droplets are uniformly distributed over the cross-section of the rig. The densification of the water phase up

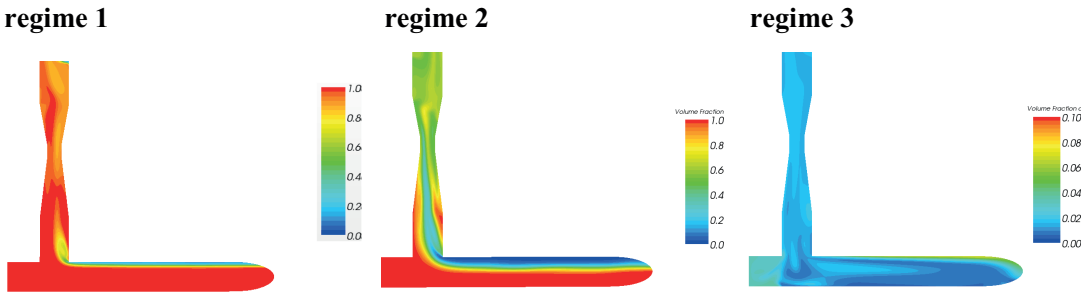

Figure 3: Time-average contours of water volume fraction in the midline cross-section of the model for regimes 1-3.

to 10% is however observed at the inlet part of the horizontal pipeline due to the lift of the water droplets in the entrance bend.

Time-average contours of the flow velocity magnitude are presented in Figure 4 for the midline cross-section of the system, regime 1-3. It generally follows from the figure that the horizontal pipeline region is associated with the uniform flow velocity profile with the average value approximately equal to the inlet value of 0.28, 0.82 and 7.49 m/s for regime 1-3 respectively. The blind-T region is the stagnation zone with the velocity minimum. The flow acceleration zone is observed for regime 1-2 in the right part of the entrance to the confuzor where the air stream is injected into the flowmeter. This local velocity maximum is established due to the occupation of region by the relatively high volume fraction of air, and, as a result, reduction of the mean flow viscosity. Similar behaviour is not detected for regime 3 where the flow is homogeneous and there are no sharp gradients of the volume fraction. The outlet of confuzor is always associated with another velocity maximum for all the regimes. There are however differences in the location of the absolute maximum in the throat of the flowmeter: shift to the region with highest air volume fraction for regime 1-2, high-speed flow stream reflection for regime 2. Due to the shift of the local velocity maximum in the throat of the flowmeter, the flow velocity profile in the diffuser becomes non-uniform.

Time-average contours of water volume fraction in the transversal cross-sections at the centre of the confuzor, throat of the flowmeter and the diffuser are presented in Figure 5 A-C for regime 1. They are combined with the time-average contours of the flow velocity presented together with the vectors of the secondary flow for regime 1 in Figure 5 D-G. The blind-T location is denoted by "T" in the figure while gravity is directed into the figure. As it follows from the figure, the local maximum of the air volume fraction (up to 20%) in the confuzor (Figure 5A) is dislocated apart from the

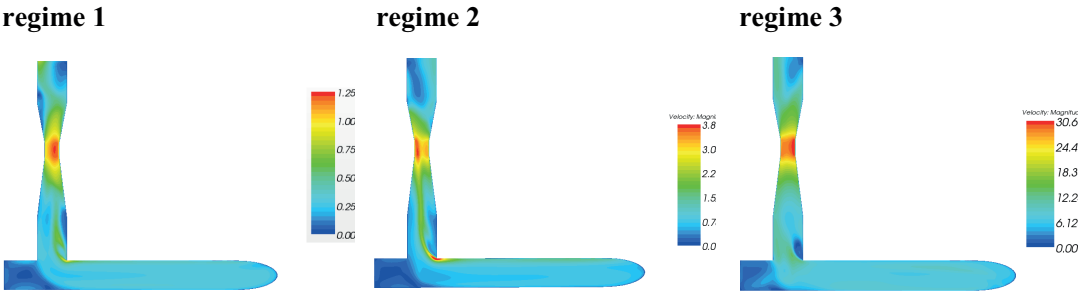

Figure 4: Time-average contours of flow velocity magnitude in the midline cross-section of the model for regime 1-3.

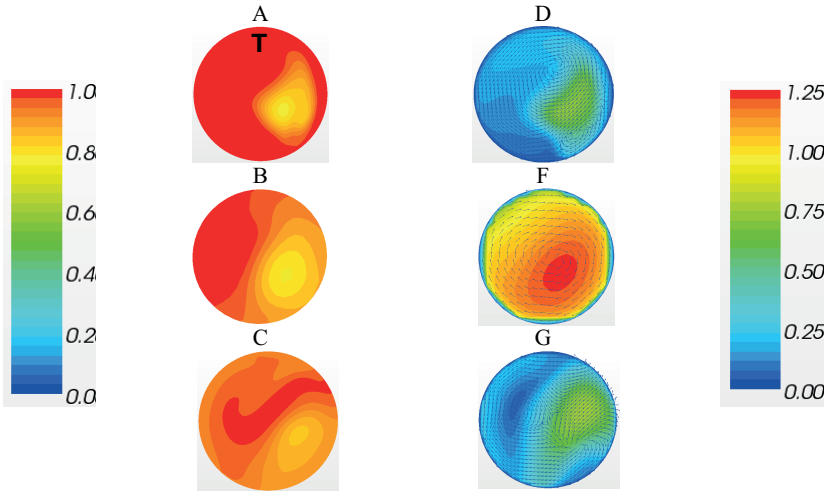

Figure 5: Regime 1. A-C: time-average contours of water volume fraction in the transversal cross-sections at the inlet (A), throat (B) and outlet (C) of the device. D-G: time-average contours of flow velocity magnitude together with vectors of secondary flow at the inlet (D), throat (F) and outlet (G) of the device. "T" designates the orientation of flow conditioner relatively to cross section. Gravity is directed into the drawing.

centre of the channel due the formation of two vortex structures of the Dean type (Figure 5D).

The maximum of the flow velocity magnitude is associated with the maximum of the air volume fraction. Since the confuzor introduces significant hydraulic resistance into the flow, the flow velocity profile in the throat of the flowmeter becomes mostly uniform for regime 1, the flow is accelerated by the confuzor. Slight shift of the velocity maximum into the right part of the cross-section could be addressed to the maximum of the air local volume fraction which conserves its position in the transition from the confuzor to the throat due to the inertia. The flow in the throat of the flowmeter is the centralized swirl flow what distributes the air widely within the cross-section. The rotation, induced in the throat of the flowmeter, in combination with the total flow deceleration in the diffuser is responsible for further detachment of the liquid phase from the walls and the dislocation of the liquid phase volume fraction maximum to the

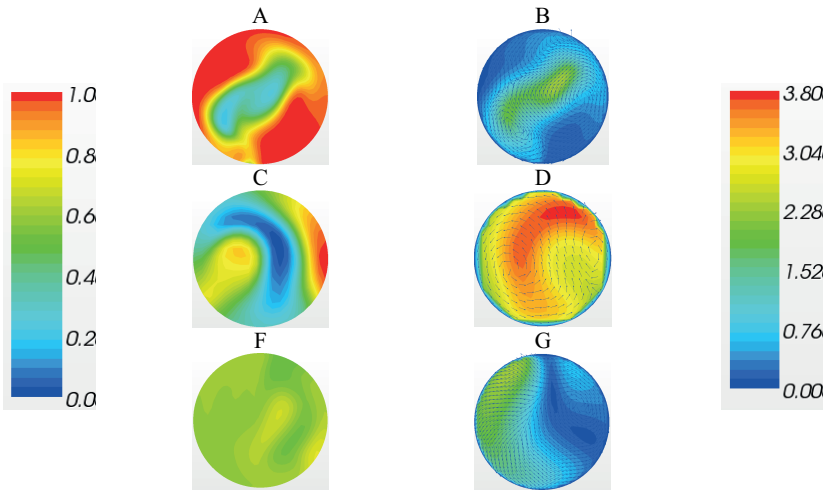

Figure 6: Regime 2. A-C: time-average contours of water volume fraction in the transversal cross-sections at the inlet (A), throat (B) and outlet (C) of the device. D-G: time-average contours of flow velocity magnitude together with vectors of secondary flow at the inlet (D), throat (F) and outlet (G) of the device. Blind-T and gravity oriented as in Fig.5.

centre of the diffuser part. The maxima of the flow velocity and the volume fraction of the air remain at approximately same position due to the higher superficial velocity of the gas phase. The vortex is however shifted into the region of the local maximum of the water phase volume fraction.

Regime 2 is considered for the same transversal cross-sections of the flowmeter in Figure 6A-G. The air volume fraction profile shown in Figure 6A for the centre of the confuzor region is of stretched elliptical shape due to the existence of two Dean-vortices centralized at the focuses of the ellipse. The volume fraction of the air in the core of the flow is up to 50%, i.e. around 10% of the rest of the air is distributed within the liquid phase. The maximum of the velocity magnitude is associated with the maximum of the air volume fraction in a fashion similar to regime 1. Contracting channel of the confuzor distributes the gas phase over the centre of the throat. Two vortex structures remain in this region due to the higher Dean number for regime 2. The intensive swirl motion is responsible for the non-uniformities in the flow velocity magnitude there; the maximum of the velocity is then shifted to the blind-T region while the entire flow velocity magnitude is increased due to contraction. The intensive mixing within the central part of the flowmeter is responsible for flow homogenisation in the diffuser region. The flow velocity profile is however slightly non-uniform in the diffuser due to the inertia of the flow so the maximum velocity region from the throat is transferred into the diffuser.

The volume fraction and velocity profiles are given for regime 3 in Figure 7A-G. The flow is mostly homogeneous all over the flowmeter. The flow velocity profile is

uniform for the confuzor part which accelerates the flow and increases the velocity magnitude in the throat of the flowmeter. The velocity profile there becomes non-uniform due to the reflection of the main flow from the confuzor wall which is associated with the blind-T that was illustrated in Figure 3. This non-uniformity is transferred into the diffuser zone.

4. Conclusions

The numerical study of the two-phase flow in the vertical flowmeter nozzle has been performed. The three-dimensional transient mixture multiphase CFD-model, coupled with the RANS k-epsilon turbulence model, was developed with the use of commercial software STAR-CCM+. The model accounts for interphase phenomena via the surface tension force. The CFD-simulations of the process elucidate important details of the flow morphology. The analysis of the phase volume fraction profiles comes out with the conclusion that the blind-T can not be considered as the perfect solution for the establishment of the homogeneous flow in the device for the investigated operational conditions. Namely, the phases become inter-mixed only at the diffuser part while the densitometer is usually placed at the flowmeter throat. The non-uniformity of flow profiles in the confuzor and the throat part of the flowmeter is governed by the combination of following factors: the relative interfacial slip, the secondary flow swirl and the refraction of the flow jet from the walls of the confuzor. It could also be noted that the Venturi nozzles, accompanied by blind-T at the entrance, could be utilized as the low-resistance flow homogenizers. The model is validated with the flow map for the vertical two-phase pipe flow, demonstrating qualitative agreement with the map.

Acknowledgements

Authors acknowledge support from the MEPhI Academic Excellence Project (Contract No. 02.a03.21.0005).

Nomenclature

C: heat capacity [J/kgK]
c_{sk}: superficial velocity [m/s]
d: pipeline diameter [m]
De: Dean number $De = Re\sqrt{d/2R}$

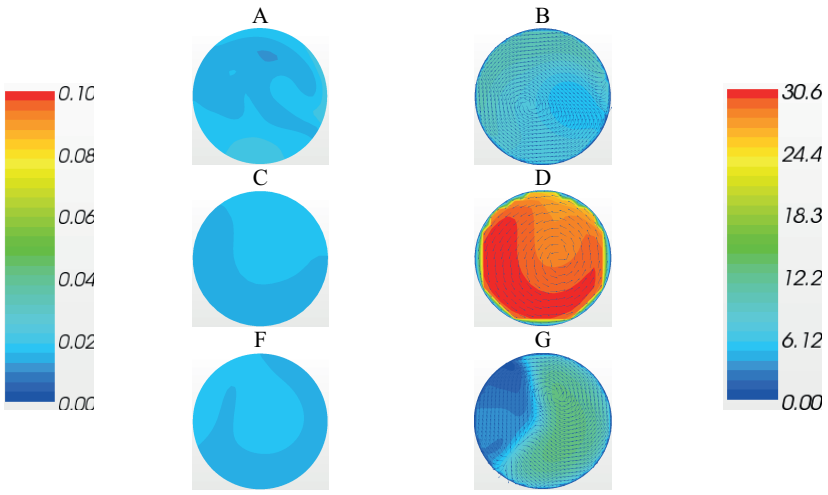

Figure 7: Regime 3. A-C: time-average contours of water volume fraction in the transversal cross-sections at the inlet (A), throat (B) and outlet (C) of the device. D-G: time-average contours of flow velocity magnitude together with vectors of secondary flow at the inlet (D), throat (F) and outlet (G) of the device. Blind-T and gravity oriented as in Fig.5.

e: energy [m^2/s^2]

F: volume flow rate [m^3/s]

f_c: capillary force per unit volume [N/m^3]

g: acceleration due to gravity [m/s^2]

k: turbulent kinetic energy [m^2/s^2]

M: molar mass [kg/mol]

N_k: velocity number $N_k = c_{sk}\left(\rho_l/g\sigma\right)^{0.25}$

p: pressure [Pa]

R: radius of the curvature [m]

Re: Reynolds number $Re = \rho_m |u| d/\mu_m$

R_u: universal gas constant [J/mol · K]

T: temperature [K]

t: time [s]

u: flow velocity [m/s]

Greek letters

ε: turbulent energy dissipation rate [m^2/s^3]

φ: volume fraction

κ: von Karman constant

μ: dynamic viscosity [Pas]

μ^t: turbulent viscosity [Pas]

ρ: density [kg/m^3]
σ: surface tension [N/m^2]

Subscripts, superscripts

g: gas
in: inlet
k: phase index
l: liquid
m: mixture
s: superficial
t: turbulent
T: transposed

References

[1] Abbas H, Lucas G (2011). Experimental and theoretical study of the gas–water two phase flow through a conductance multiphase Flowmeter meter in vertical annular (wet gas) flow. Nuclear Engineering and Design 241:1998–2005.

[2] Amini A, Schleiss AJ (2009). Numerical modeling of oil-water multiphase flow contained by an oil spill barrier. Engineering Applications of Computational Fluid Mechanics 3:207-219.

[3] Balakin BV, Hoffmann AC, Kosinski P, Høiland S (2010). Turbulent flow of hydrates in a pipeline of complex configuration. Chemical Engineering Science 65:5007-5017.

[4] Corneliussen S, Couput J.-P, Dahl E (2005). Handbook of Multiphase Flow Metering, 2nd Ed., NFOGM/Tekna, Oslo, Norway.

[5] Helland K (2004). Gas Technology: treatment and production of natural gas, Bergen University College (in Norwegian).

[6] International Organization for Standardization: Measurement of Fluid Flow by Means of Pressure Differential Devices Inserted in Circular Cross-Section Conduits Running Full, ISO 5167:2003.

[7] Kuo JT, Wallis GB (1988). Flow of bubbles through nozzles. International Journal of Multiphase Flow 14:547-564.

[8] Jana AK, Das GP, Das K (2008). The hydrodynamics of liquid–liquid upflow through a flowmetermeter. International Journal of Multiphase Flow 34:1119–1129.

[9] Lupeau A, Platet B, Gajan P, Strzelecki A, Escande J, Couput J-P (2007). Influence of the presence of an upstream annular liquid film on the wet gas flow measured by a Flowmeter in a downward vertical configuration. Flow Measurement and Instrumentation 18:1-11.

[10] Malayeri MR, Smith JM, Steinhagen H (2001). The behaviour of gas–liquid and vapour–liquid upward bubbly flows passing through a vertical Flowmeter. Transactions of IChemE 79:371–375.

[11] Oddie G, Pearson JRA (2004). Flow-rate measurement in two-phase flow. Annular Review of Fluid Mechanics 36:149–172.

[12] Paladino EE, Maliska CR (2002). Multi-phase flow modelling in differential pressure flow meters. 9th Brazilian congress of thermal engineering and sciences, CIT02-007.

[13] Patankar NA, Joseph D (2001). Modeling and numerical simulation of particulate flows by the Eulerian–Lagrangian approach. International Journal of Multiphase Flow 27:1659–1684.

[14] Viswanathan S (1998). Development of a pressure drop model for a variable throat flowmeter scrubber. Chemical Engineering Journal 71:153–160.

[15] Wehinder GD, Peeters J, Muzaferija S, Eppinger T, Kraume M (2013). Numerical simulation of vertical liquid-film wave dynamics. Chemical Engineering Science 104: 934-944.

[16] Xu K, Zhou W, Li X (2012). Wet gas flow modeling for a vertically mounted Flowmeter meter. Measurement Science and Tehcnology 23:045301.

[17] Zhou L, Liu De-y, Ou C-qi (2011). Simulation of flow transients in a water filling pipe containing entrapped air pocket with VOF model (2011). Engineering Applications of Computational Fluid Mechanics 5:127-140.

[18] http://www.aalto.ca/aaltoinc/Datasheets/EH5053W.pdf

[19] http://www.controlswarehouse.com/sheets/endress/endress_prowirl_77_spec.pdf

[20] https://www.honeywellprocess.com/library/marketing/tech-specs/34-ST-03-60.pdf

[21] http://support.casio.com/en/manual/001/EXFH25_M10_FB_EN.pdf